Reconstruction and roughening of a catalytic Pt(110) surface coupled to kinetic oscillations

Michael Monine and Len Pismen

Department of Chemical Engineering, Technion, 32000 Technion City, Haifa, Israel
and Minerva Center for Nonlinear Physics of Complex Systems and Institute of Catalysis Science and Technology, Technion, Israel
(Received 2 July 2002; published 5 November 2002)

Three-dimensional reconstruction and roughening of a Pt(110) surface is studied with the help of a qualitative Monte Carlo model. A distinct CO adsorption uptake on different surface phases is taken into account. The computations show that a ''missing row'' structure with defects relaxes to a more stable (111)-faceted structure. The $CO+O_2$ reaction kinetics is modeled by a phenomenological equation with a cubic nonlinearity reproducing a correct qualitative picture of oscillations. The surface roughening developing under the reaction conditions causes slow changes in catalytic activity of the surface. A nanoscale front between the 1×1 and 1×2 phases disintegrates due to repeated phase transitions caused by CO coverage oscillations. Defect formation and roughening dominate the dynamics of surface phase transitions. A one-dimensional extension of the model reproduces microscopic traveling waves on the CO diffusion scale.

I. INTRODUCTION

Catalytic reactions on oriented single crystals often exhibit rate oscillations and produce a variety of spatiotemporal patterns on the μm scale [1]. The most thoroughly studied system of this kind is CO oxidation on Pt(110) [1–4]. The mechanism of rate oscillations and pattern formation in CO $+O_2$/Pt reaction under low pressure isothermal conditions is based on an adsorbate-induced surface phase transition controlled by the CO coverage.

It is well known that (110) and (100) surfaces of many transition metals undergo reversible surface reconstruction [5] which can be lifted by some adsorbates, e.g., CO or NO [6–9]. The reconstruction reduces the surface energy of a clean (110) surface of a face-centered cubic (fcc) lattice of such metals as Rh, Pd, Ir, Pt, Au, Ag, etc., by creating the ''missing row,'' or 1×2 structure with the sides of the rows forming (111) facets. Since the (111) structure is characterized by lower surface free energy, the geometries exposing the most extensive (111) facets are favored [10–12]. Higher-order $1\times n$ superstructures are favored as well, in as much as they exhibit (111) facets [10].

The reconstruction is lifted at high CO coverage. The restored 1×1 structure has higher catalytic activity, mainly due to a larger oxygen sticking coefficient. The reaction reduces the CO coverage, prompting reconstruction, etc. The adsorbate plays the role of a fast global activator in a common oscillation and pattern formation mechanism, while the phase transition responsible for changes in catalytic activity plays the role of a slow inhibitor. Since both $1\times1\rightarrow1\times2$ reconstruction and its reverse involve mass transport, repeated transitions accompanying kinetic oscillations may lead to roughening and faceting of an originally flat surface. This, in turn, may cause slow changes in average catalytic activity observed in the experiment [13–18].

A number of more or less realistic phenomenological mean-field (MF) models based on reaction-diffusion (RD) systems have been developed during the last decade in order to describe microscopic spatiotemporal patterns in catalytic reactions [19–31]. Simulation of pattern formation in the $CO+O_2$/Pt(110) reaction with the help of a realistic RD model [20] reproduced spiral waves patterns under oscillatory, excitable, and bistable conditions. Phenomenological models of the FitzHugh-Nagumo type reproduced qualitatively target patterns [21] and spirals of different shapes in NO reduction on Rh(110) surface [22], as well as traveling wave fragments in excitable media [23]. In all these models spatial coupling was introduced through adsorbate surface diffusion, including also effects of surface anisotropy [22,23].

A somewhat different approach was taken in models based on the dynamics of fronts in systems with separated spatial scales, including the transition between Ising Bloch fronts [25–27] and taking into account effect of front curvature [28–30]. Generally, a front is defined as a boundary between two stable or metastable states of a short-scale field variable set into motion under the action of a long-range controlling field variable. The commonly used models include a long-range inhibitor shifting the equilibrium between the two competing states of a short-scale activator. Due to the large scale separation, the equation of the short-scale variable can be replaced by a kinematic equation of boundary dynamics (BD) for the normal speed of the front depending on the local value of the long-range variable as well as the curvature. This method has been applied to model labyrinth patterns [29] and islands dynamics on a roughened surface [30]. The BD method is also applicable to strongly anisotropic surfaces [31].

Neither usual MF models nor BD method are able to resolve the local dynamics of surface reconstruction and take into account surface roughening and faceting, which may strongly affect catalytic activity [13–18]. This prompted the interest to application of Monte Carlo (MC) techniques allowing us to elucidate nanoscopic effects of surface reconstruction [32,33]. Imbihl *et al.* [32] reproduced qualitatively the development of a regular facet structure due to the surface restructuring on Pt(110) during CO oxidation with the help of a one-dimensional (1D) MC model. Experimentally, the faceting is observed within a certain range of CO pressures p_{CO}, and leads to an increase in catalytic activity [13–

18. The 1D model has, of course, severe limitations, since only 1D interactions between nearest neighboring (NN) sites can be included.

MC simulations of the $1\times2\rightarrow1\times1$ transition caused by CO adsorption were carried out by Thostrup *et al.* [33] using realistic values of the energies of Pt-Pt interactions; the results compared well with scanning tunnel microscope (STM) observations. Another MC model extended to micro-scale [34] described explicitly the adsorbate dynamics and kinetics of CO oxidation, but accounted for the $1\times1\rightleftharpoons$ hex reconstruction on Pt(100) just by tagging the surface sites. This model generated spatiotemporal patterns even without the inclusion of CO diffusion, as the reaction-driven front removed the adsorbates from NN adjacent sites and caused surface phase transition and local synchronization of oscillations. Zhdanov and Kasemo [35] simulated explicitly both the reversible $1\times2\rightleftharpoons1\times1$ reconstruction on a 2D lattice and adsorbate dynamics. The displacement of both Pt atoms and adsorbate was governed by a Metropolis rule [36,37]. The probabilities of the elementary steps, such as CO and O_2 adsorption and desorption, O_2 dissociation and CO+O reaction, were deduced from macroscopic data, and the energies of Pt-Pt interactions were similar to those used in Ref. [33]. The reconstruction model included, however, only motion in a 2D plane and did not take into account 3D roughening effects.

The aim of this communication is to give a qualitative Monte Carlo model describing dynamics of Pt(110) surface reconstruction and 3D roughening and faceting under reactive conditions on atomic scale. The model, described in detail in Sec. II, accounts explicitly for 3D motion of Pt atoms but treats the more diffusive adsorbate as a global variable averaged over surface nanodomains. We first apply this model in Sec. III to the study of equilibrium surface structure and relaxation following a step change of adsorbate coverage. Next, we describe in Sec. IV the dynamics of roughening coupled to kinetic oscillations on a nanodomain with the adsorbate coverage constant in space. We use phenomenological kinetic equation of the time-dependent Ginzburg-Landau (TDGL) type, which is known to give a correct qualitative picture of oscillations. We show in Sec. V that fronts between 1×1 and 1×2 phases do not persist on an atomic scale but disintegrate due to surface roughening. In Sec. VI we extend our nanoscale model to larger scales including the adsorbate diffusion, and show that spatial synchronization of chemical oscillations leads to formation of propagating waves with the wavelength commensurate with the adsorbate diffusion range.

A more realistic kinetic Monte Carlo (KMC) [37] simulations taking into account distinct activation barriers for elementary atomic jumps and using realistic adsorbate dynamics will be described in a future communication. KMC simulations consume much more computer time because realistic transition rates for slow and fast process may differ by 7–10 orders of magnitude [38]. Our preliminary data suggest that the effects of reaction-induced roughening obtained here with the help of a simple phenomenological model are retained qualitatively also in KMC computations.
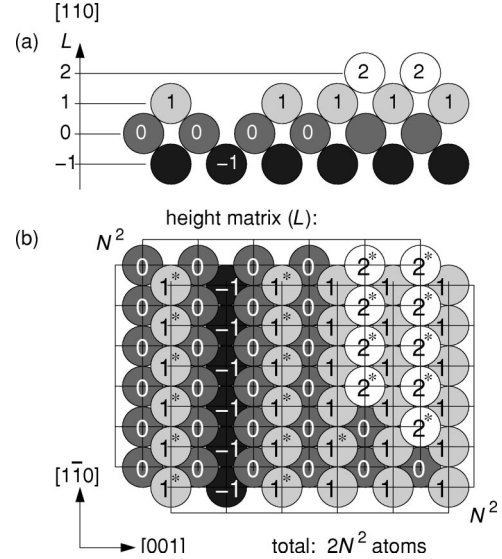

FIG. 1. Representation of the Pt(110) surface. (a) $[1\bar{1}0]$-section of a roughened (110) surface. (b) The surface relief is characterized by the matrix of heights of top sites (integer numbers). Free top atoms marked by an asterisk are allowed to move.

II. THE MODEL

By our definition, the (110) surface of a fcc lattice consists of $2N^2$ nodes; each of them is marked by an integer L defining the upper occupied level, as shown in Fig. 1. Only atoms occupying free top sites (i.e., not covered by any neighboring atom in the higher layer) are allowed to move. Their total number never exceeds N^2; the upper limit corresponds to the regular 1×1 structure. It is assumed that the atomic structure has no overhangs, i.e., each surface atom is always based on four occupied sites in the layer below. More details can be found in Ref. [39]. The energy of the surface atoms is assumed to be dependent on the occupancy of the four nearest sites in the same layer:

$$E=\sum_i n_i E_i, \tag{1}$$

where the index i denotes the "vertical" and "horizontal" NN positions ($i=v,h$) and E_i is the Pt-Pt binding energy between NN atoms. The vertical and horizontal directions are parallel to $[1\bar{1}0]$ and $[001]$ axis, respectively. The difference between E_v and E_h accounts for the anisotropy of the (110) plane. A positive E_h makes 1×2 reconstruction energetically favorable, whereas the 1×1 structure becomes preferred when E_h decreases below zero.

The general dependence of binding energies on CO coverage (θ) reads,

$$E_i=e_i+q_i(\theta), \tag{2}$$

where e_i is ith energy component for the clean 1×2 surface and the function $q_i(\theta)$ accounts for the repulsive action of CO molecules adsorbed on pairs of NN top atoms. We assume that CO molecules migrate rapidly between adjacent NN top sites. This allows us to use a mean-field approxima-
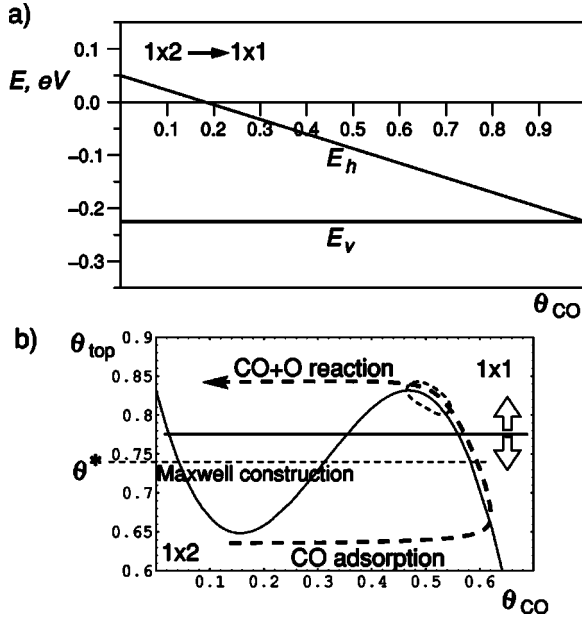
FIG. 2. (a) The linear dependence of NN-interaction energies on CO coverage θ. (b) The nullcline of Eq. (6) showing an adsorption-reaction hysteresis. The level θ^* denotes the Maxwell construction. (Coexistence of the two phases is kinetically unstable.)

tion for CO coverage. It is well known that CO adsorption destabilizes the 1×2 state favoring the 1×1 structure. This can be modeled by making E_h a decreasing function of the surface-averaged CO coverage θ, while keeping E_v constant. As saturation CO surface coverage is reached, E_h tends to be close to E_v, so that 1×1 patches are almost isotropic [33]. Taking into account the fact that CO sticking probabilities on different surface configurations are not the same [33], we assume the following linear dependence of the interaction energies on θ:

$$E_i = e_i + q_i \times \begin{cases} \theta_{1\times1}^{\mathrm{CO}} & \text{on } 1\times1 \text{ phase} \\ \theta_{\mathrm{rest}}^{\mathrm{CO}} & \text{on the rest of configurations,} \end{cases} \quad (3)$$

with

$$\theta_{1\times1}^{\mathrm{CO}} = \theta[\theta_{1\times1} + (1-\theta_{1\times1})/k]^{-1} \quad \text{and} \quad \theta_{\mathrm{rest}}^{\mathrm{CO}} = \theta_{1\times1}^{\mathrm{CO}}/k, \quad (4)$$

where $\theta_{1\times1}^{\mathrm{CO}}$ and $\theta_{\mathrm{rest}}^{\mathrm{CO}}$ are CO coverages on 1×1 phase and the rest of the configurations, respectively; θ is the total CO coverage, $\theta_{1\times1}$ is the surface fraction of 1×1 phase and the ratio $1/k$ describes a relative uptake of CO on the 1×2 patches and defects. The values used in the following computations are $e_v = -0.225$ eV, $e_h = 0.05$ eV, $q_v = 0$ eV, $q_h = -0.275$ eV. The values of e_v and e_h were chosen to be close to those used by Thostrup et al. [33]. We have fitted q_v and q_h in order to obtain the onset of $1\times2\rightarrow1\times1$ reconstruction when θ reaches the critical value $\theta_{cr}\approx0.25$, in accordance with the experiment [9]. The linear dependence of E_v and E_h on θ is shown in Fig. 2(a). The transition probabilities for surface atoms are calculated according to the Metropolis rule [36]

$$W_i = \min\left\{\exp\left(-\frac{\Delta E_i}{k_B T}\right), 1\right\}, \quad (5)$$

where ΔE_i is the energy difference between the new and old positions, k_B is the Boltzmann constant [eV/K] and T is the temperature. Activation energies are not taken into account, which actually implies that all possible transitions are assumed to have identical activation energies. The reconstruction attempts are carried out in the following sequence: (i) a random upper-layer atom is selected on the lattice by using a congruential generator of uniformly distributed pseudorandom numbers [37,40]); (ii) for the chosen free atom, possible transition sites are determined; (iii) the transition is executed with the probability defined by Eq. (5). The number of attempts equal to the lattice dimension, $2N^2$, is called a Monte Carlo step (MCS).

A realistic mean-field model of the $CO+O_2/Pt(110)$ reaction contains three dynamic variables describing the coverages of CO, atomic oxygen and active (1×1) phase [9]. Nevertheless, only CO adsorption is known to be important for the surface reconstruction. The reconstruction process limits the catalytic activity of the surface, while the oxygen adsorption, dissociation as well as chemical reaction occuring on active surface patches can be considered as relatively fast processes. We focus our atention on the reconstruction problem and, for the sake of simplicity, replace the realistic chemical kinetics by a TDGL equation which reproduces a correct qualitative picture of oscillations. Therefore, rather than solving two ordinary differential equations including CO and O_2 adsorption/desorption, O_2 dissociation and chemical reaction terms, we will use a single equation for a global variable v of the same form as in Ref. [21]:

$$\frac{1}{\gamma'}\frac{\partial v}{\partial t} = v - v^3 - \eta, \quad (6)$$

where γ' is a time scale ratio. The variable v models action of the CO adsorbate lifting the $1\times2\rightarrow1\times1$ reconstruction and plays a role of "fast activator." The oxygen coverage is slaved to the CO coverage and therefore its action is not included explicitly. Equation (6) has two stable stationary states biased by the level of a "slow inhibitor," which is defined here in such a way that the level $\eta=0$ corresponds to the Maxwell construction. We interpret it here as a surface state variable that models adsorption and catalytic properties of the surface. The multiplicity region in Eq. (6) lies within the interval $-2/\sqrt{3}\leqslant v\leqslant 2/\sqrt{3}$, therefore, the correspondence to the actual CO coverage is established through the relation $v=2/\sqrt{3}(\alpha\theta-1)$. We define the feedback of the surface structure through the fraction of active top sites by setting in Eq. (6) $\eta=\beta(\theta_{\mathrm{top}}-\theta^*)$. This introduces a bias in favor of the low-coverage state due to chemical reaction when the fraction of active top sites θ_{top} is high, and in favor of the high-coverage state (due to CO adsorption) when θ_{top} is low. In the ideal case we would have $\max(\theta_{\mathrm{top}})=1$ (N^2 free top atoms) on the 1×1 surface and $\min(\theta_{\mathrm{top}})=0.5$ ($N^2/2$ free top atoms) on the 1×2 surface. Then the level $\eta=0$ should correspond to $\theta^*=0.75$ and the constant
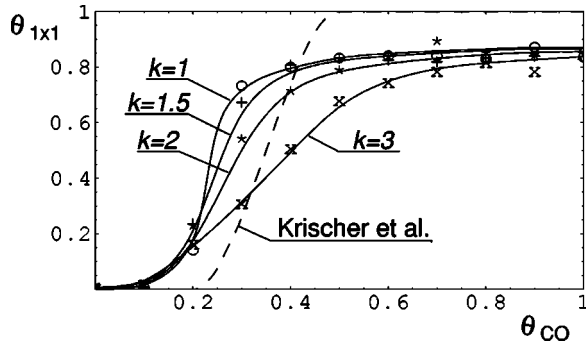
FIG. 3. Dependence of the equilibrium 1×1 fraction on CO coverage simulated at varied values of CO uptake ratio k. For comparison, the steady-state dependence of $\theta_{1\times1}$ on θ obtained from the surface phase transition model of Krischer *et al.* is shown by the dashed line.

β should be equal to $8/(3\sqrt{3})$. Since, however, the surface structure has many defects, θ_{top} never reaches either 0.5 or 1. The variation range $\Delta\theta_{top}$ is less than 0.5, therefore, it is appropriate to choose $\theta^* < 0.75$, $\alpha > 2$, and $\beta > 8/(3\sqrt{3})$, e.g., $\theta^* = 0.74$, $\alpha = 3.2$, and $\beta = 4.2$. Figure 2(b) illustrates the nullcline of Eq. (6) and the hysteretic relaxation between the two states.

We solve numerically the following equation:

$$\gamma^{-1}\frac{\partial\theta}{\partial t} = \frac{2}{\sqrt{3}}(2\theta-1) - \frac{8}{3\sqrt{3}}(2\theta-1)^3 - a(\theta_{top}-\theta^*),$$
(7)

with $\gamma = \gamma'\sqrt{3}/4$. The constant γ characterizes the reaction rate. In the following computations we choose $\Delta t = 0.01$ and vary γ. The variable θ_{top} is averaged over the entire nanodomain surface.

The computations have been carried out in the following sequence: (i) executing 1 MCS $= 2N^2$ attempts on the atomic lattice using θ from the previous time step to calculate the transition probabilities; (ii) solving Eq. (7) on the next time step using the data on the surface relief and CO fractions from the previous time step; (iii) computing statistical characteristics of the surface data (θ_{top} and dispersion) to be used in the next iteration. The following computations have been carried out on the nanodomain lattice consisting of 2×50^2 atoms.

The surface roughening is measured by the variance of top occupied lattice sites, $\langle L_i^2 \rangle - \langle L_i \rangle^2$, where $i = 1, \ldots, 2N^2$. The variance is equal to 0.25 and 0.5 for the ideal 1×1 and 1×2 structures, respectively.

III. SURFACE RELAXATION

We investigate first the equilibrium surface structure. The saturation curves shown in Fig. 3 have been obtained from long run computations at different values of CO coverage θ and uptake ratio k. At $\theta < 0.1$ the 1×2 state covers the surface. Small patches of the 1×1 phase nucleate at $\theta \sim 0.2$. Further increase of θ leads to the formation of large islands of the 1×1 phase coexisting with the 1×2 patches and de-

fects. The phase coexistence interval extends to higher CO coverages at larger values of the parameter k. At $\theta > 0.6$, the 1×1 phase prevails. The fraction of 1×1 phase is calculated as $\theta_{1\times1} = n_{1\times1}/N^2$, where $n_{1\times1}$ is the number of atoms in a close-packed configuration, i.e., those having eight nearest neighbors. Boundary atoms are not counted; therefore, the maximum value of $\theta_{1\times1}$ is about 0.85. The simulations of the surface relaxation indicate that the 1×2 surface with defects may be unstable. At low temperatures ($T \sim 350$ K) the 1×2 surface shown in Figs. 4(a), 4(b) is thermodynamically stable. An increase of temperature ($T \sim 1100$ K) causes the relaxation of a relatively flat 1×2 surface to the (111)-faceted $1\times n$ superstructure shown in Figs. 4(a), 4(d). The dynamics of this transition is presented in Figs. 4(c), 4(e). The available data [11] suggest that $1\times n$ superstructures are more stable than the 1×2 surface, but the conditions causing such higher-order reconstructions involve some more complicated treatment, e.g., heating in an oxygen atmosphere. At the same time, experimental studies show that at high T (about 1025 K) a well-ordered 1×2 surface undergoes a roughening transition to disordered state. This transition cannot be described without taking into account activation barriers for atomic jumps in our model. Introducing activation energies will prevent fast reconstruction to the stable (111)-faceted structure blocking the following reconstruction.

IV. OSCILLATIONS AND ROUGHENING

Since repeated phase transitions accompanying kinetic oscillations involve mass transport, it is natural to expect an increase of roughening during the oscillations. This is, indeed, confirmed by the computations presented below. The roughening occurs as a result of the reverse $1\times1\rightarrow1\times2$ transformation initiated by a fast decrease of CO consumed by the reaction. The Pt atoms blocked by CO in the close-packed 1×1 configuration at high θ hop to the layer above as soon as the reaction removes CO from the surface. The hopping occurs most easily on those atomic configurations where only one $(1\bar{1}0)$ NN pair exists, i.e., at boundaries of 1×1 domains. Atomic steps formed at the initial stage of such a transition are distributed in an irregular way along the boundary, but further decrease of CO favors formation of atomic rows in the $(1\bar{1}0)$ direction, leading to the formation of a $1\times n$ surface structure. The lowest energy state is reached when the number of (001) NN pairs of Pt atoms is reduced to a minimum. When CO covers the surface again, it shifts a part of the top Pt atoms to the layer below to form the 1×1 structure which has more capacity for CO adsorption. Single Pt adatoms remaining on the upper layer migrate chaotically on the quasistable 1×1 surface and merge in clusters. Thus, chemical oscillations cause formation of terraces on the surface.

As new atomic layers are built onto the terraces, the surface relief develops pyramid-shaped hills. Mobility of the atoms forming the hill slopes is strongly restricted, and therefore they are not involved in the reconstruction. Thus, the regime of oscillations changes with the development of 3D surface roughening. More ordered pyramid structure can
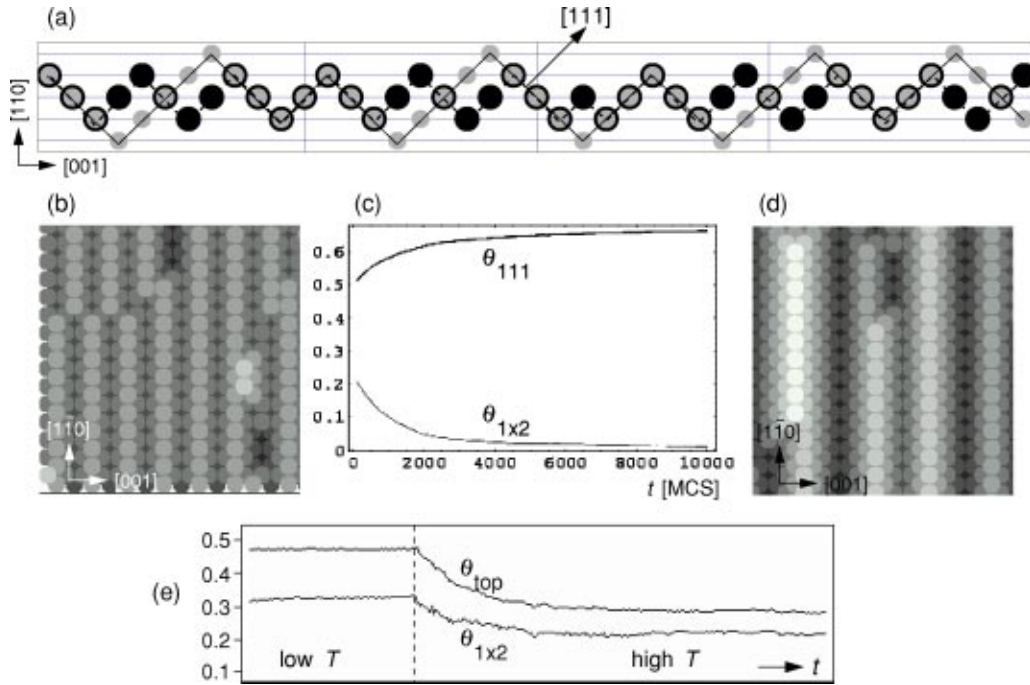
FIG. 4. Relaxation of the 1×2 surface. (a) A $[1\bar{1}0]$ section showing the 1×2 structure (black circles) and $1 \times n$ superstructure (gray circles) with a larger area of (111) facets. (b) and (d) fragments of the 1×2 and $1 \times n$ surfaces. (c) and (e) a $1 \times 2 \rightarrow 1 \times n$ transition caused by an increase of temperature T. The fraction of (111) facets θ_{111} increases while the fraction of the top $[1\bar{1}0]$-oriented rows θ_{top}, $\theta_{1 \times 2}$ decreases.

form spontaneously, with the pyramid sides consisting of stable (111) facets parallel to $(1\bar{1}0)$ axis.

The development of roughening depends on the reaction rate. When the reaction rate is relatively slow ($\gamma \sim 1$) the oscillation period fluctuates randomly and does not show a tendency to regular growth, while the oscillation amplitude decreases. In the case of a high reaction rate ($\gamma \gg 1$), the amplitude remains large but the oscillation period tends to grow with increasing roughening. At $k=1$, the roughening increases gradually with time at any values of γ; the active surface area decreases, and eventually the oscillations stop [Figs. 5(a), 5(b)]. The oscillations dynamics is sensitive to the fraction of top sites involved in the reconstruction process. A terraced surface obtained after the halt of oscillations is shown in Fig. 6. The final state fluctuates close to the right hand side extremum of the nullcline [Fig. 2(b)]. Increasing the parameter k extends the bistability region, as shown in Fig. 3. At $k=1.5$, 2, and 3, the oscillations do not stop; the roughening remains relatively low and fluctuates about average levels depending on k [Fig. 5(c)]. No oscillations were obtained at larger k.

At $k=1$ the variance grows continuously even after the halt of oscillations [Fig. 5(c)]. This result disagrees with the experimental observations and calculations of Imbihl *et al.* [18,32]. This contradiction can be resolved in KMC calculations [38] where activation barriers for atomic jumps are assigned.

V. NANOSCOPIC FRONT DISINTEGRATION

If the initial conditions include a sharp boundary between the 1×1 and 1×2 phases, spreading of a more stable state

through a front propagation would be expected in a MF model. MC computations show, however, that the front disintegrates due to effects of roughening. Figure 7 shows a sequence of frames captured at different time moments during externally imposed stepwise changes of θ. The first frame shows coexisting 1×1 and 1×2 patches separated by the front when CO coverage is about the Maxwell construction value $\theta = 0.3$ [see Fig. 2(b)]. The simulations are carried out at a sufficiently low temperature in order to prevent nucleation of defects inside the 1×2 phase and the further reconstruction through a ''hole eating'' mechanism. Thus, the two phases, as well as the front between them are stable in mean-field approximation.

A decrease of θ (frame 2) causes the boundary atoms to hop to the higher layer. This initiates a fingerlike structure propagating along the $[1\bar{1}0]$ direction. The following increase of θ (frame 3) causes formation of disordered 1×1 clusters, and the rows of the 1×2 phase merge near the front. The frames 4 to 7 in Fig. 7 show further front disintegration under successive changes of θ. Such an instability of the front leads to a strong increase of roughening. Figure 8 illustrates the atomic transport between the upper surface layers. The variance measures the dispersion of atoms between different layers averaged along the [001] direction. The labels in Fig. 8 mark the curves in accordance to the frames in Fig. 7.

The simulations show that the interphase front disintegrates during the oscillations. Since the number of top atoms on 1×1 phase is twice that on 1×2 phase, the phases cannot propagate without forming defects. Propagation of the 1×2 phase recovering the 1×1 surface and keeping 1×2 order
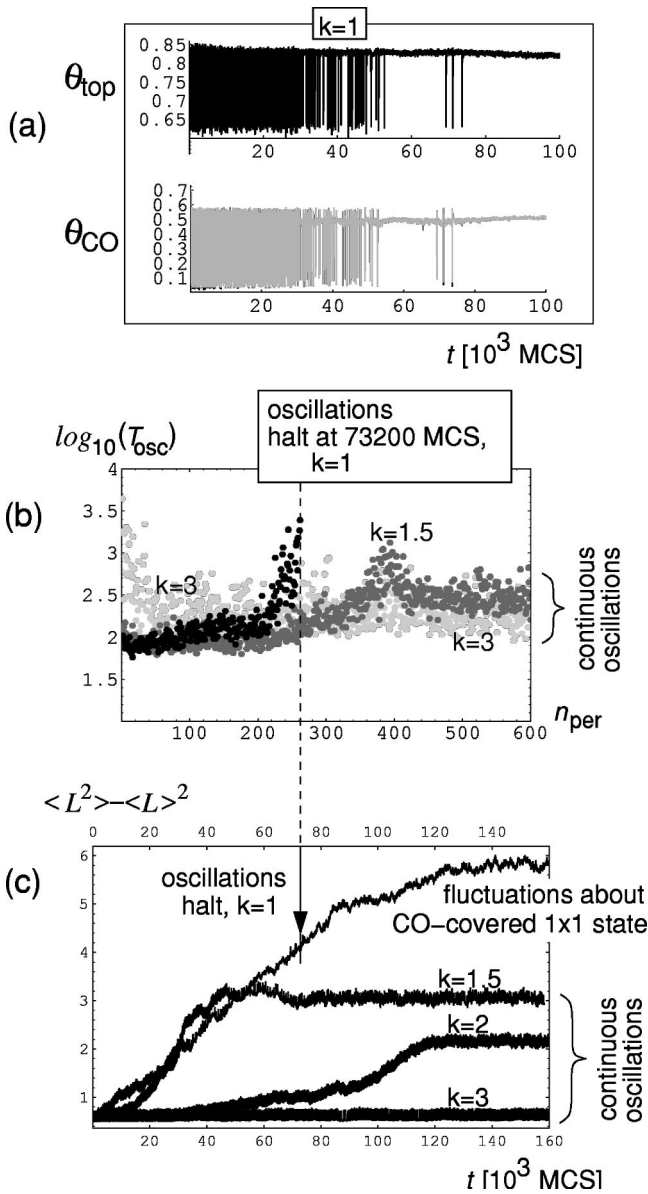
FIG. 5. (a) Oscillations at $\gamma=10$ and $k=1$. The oscillation period increases prior to a halt of oscillations at about 73 200 MCS. (b) The logarithm of the oscillation period vs the number of cycles at various k. (c) The development of surface roughening at different k. The time moment when the oscillations stop is marked by an arrow.

beyond the front is impossible due to the mass balance at the front. The phase propagation results from nucleation near defect locations and local reconstruction inside the majority phase. All of the above is true for any configuration of the front separating the 1×2 and the 1×1 phases, but at high θ a front parallel to $[1\bar{1}0]$ axis is more stable than that oriented perpendicularly to the $[1\bar{1}0]$ axis.

VI. WAVES ON MICROSCALE

In order to take into account the effect of microscopic CO diffusion, the system has been extended spatially in one di-
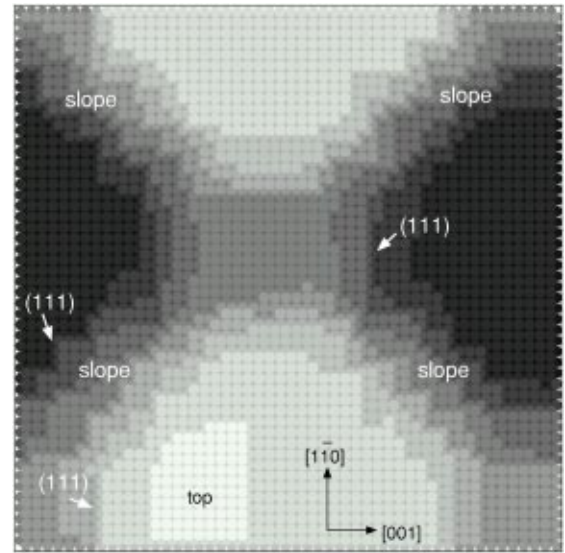

FIG. 6. A roughened surface obtained after the halt of oscillations at $\gamma=10, k=1$. The simulated area consists of 2×50^2 atoms. (The lattice scale ratio $1/\sqrt{2}$ is not preserved in this and the following figures.)

rection. We define a set of nanodomains $(i=1,\ldots,n_d)$, where each ith nanodomain is described by the average fractions of CO and top sites (θ_i and $\theta_{top,i}$). All assumptions specified before are valid for the extended model. The reconstruction attempts proceed uniformly on the entire surface area, but the respective transition probabilities depend on the CO coverage inside the particular nanodomain. Thus, there is no need of boundary conditions between the domains inside the simulated area. Periodic boundary conditions have been used only at the edges.

The governing equation reads:

$$\gamma^{-1}\frac{\partial\theta}{\partial t} = \frac{2}{\sqrt{3}}(2\theta-1) - \frac{8}{3\sqrt{3}}(2\theta-1)^3 - a(\theta_{top}-\theta^*)$$

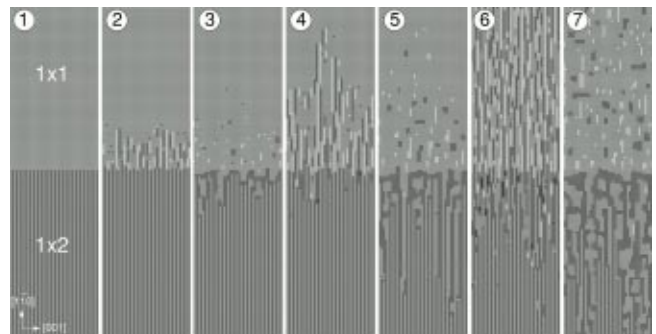$$+ D\frac{\partial^2\theta}{\partial x^2}, \tag{8}$$

FIG. 7. A series of snapshots showing disintegration of a ''perpendicular'' front caused by stepwise change of CO coverage. (1) A sharp boundary between the alternative phases coexisting at $\theta=0.3$. (2,4,6): propagation of the 1×2 phase at low θ. (3,5,7): propagation of the 1×1 phase at high θ.
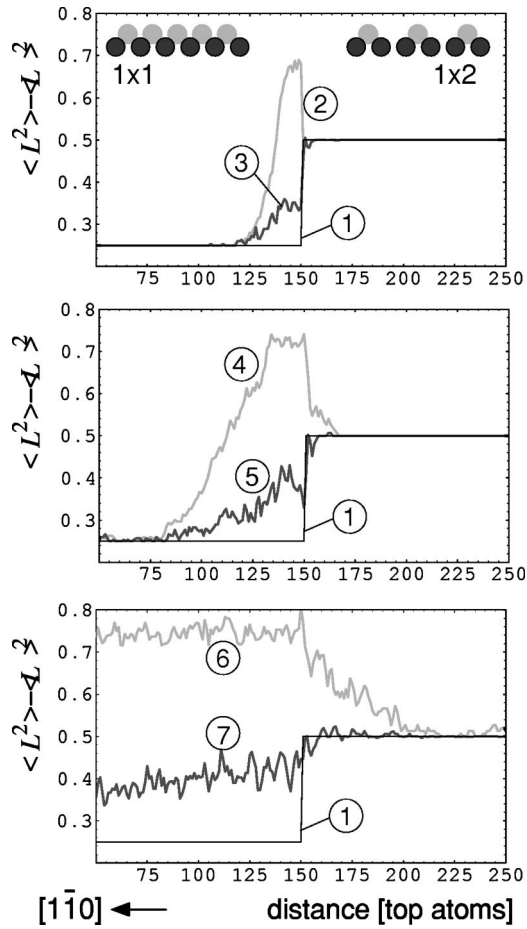
FIG. 8. The variance of top occupied lattice sites averaged along the [001] axis. The numbers at the curves correspond to the snapshots in Fig. 7.
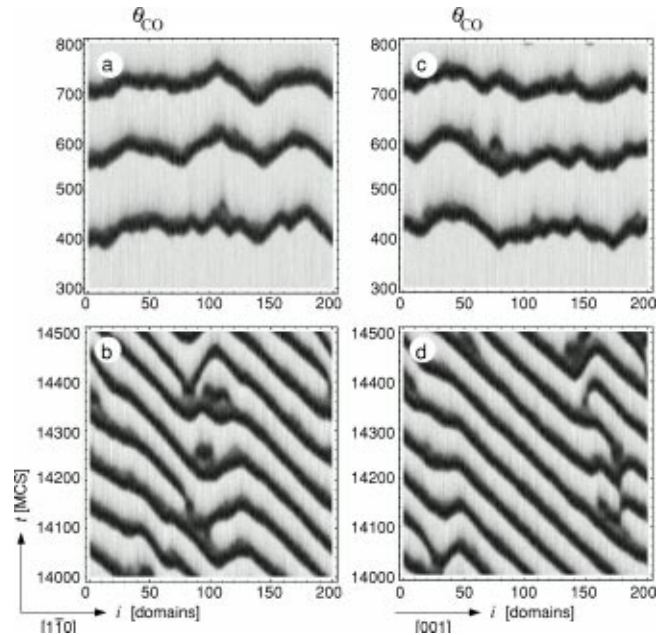

FIG. 9. Spacetime plots of traveling waves in the 1D simulation. Black areas correspond to low CO coverage ($\theta \approx 0.05$) and bright areas correspond to high ($\theta \approx 0.55$). Coefficients used in the simulation are $\gamma = 10$, $D = 3$.

where D is the CO diffusivity on microscale. We solve Eq. (8) by means of an implicit scheme [40]. The adsorbate variable θ is discretized on a grid of n_d nodes. A single nanodomain consists of $2N^2$ atoms, so that 1 MCS $= 2N^2 n_d$.

The simulations started from random initial conditions (a uniform random distribution of top atoms with $\langle L^2 \rangle - \langle L \rangle^2 \approx 0.5$). The grid consisted of 200 nanodomains, each containing 2×50^2 atoms. The Pt lattice constant along the [1$\bar{1}$0] axis is 2.77 Å [7] and the lattice scale ratio is $\sqrt{2}$. Thus, a single nanodomain measures ~ 14 nm$\times 20$ nm and the estimated length of the simulated area extends to about 2.8 μm in the [1$\bar{1}$0] direction, or to about 4 μm in the [001] direction.

Figure 9 shows the development of 1D waves in the models extended in [1$\bar{1}$0] (a),(b) and [001] (c),(d) directions. The (x,t)-contour plots of the CO coverage for the full set of nanodomains illustrate spontaneous formation and propagation of chemical waves. At the initial stage, one sees uniform oscillations starting after 400 MCS [snapshots (a),(c)]. At the following stage, oscillations in single nanodomains tend to desynchronize, but synchronization between neighboring nanodomains is maintained due to the microscale CO diffusion. This leads to the formation of traveling waves seen in Figs. 9(b), 9(d). The waves eventually split and run in two

opposite directions with the same constant speed up to a collision point. Since the periodic boundary conditions have been used, the wave traveling to the left appears in the right side of the simulated area. The same diffusivity has been used in both computations. The propagation speed and wavelengths are insensitive to the surface anisotropy. This finding agrees with the conclusions presented in Ref. [2] and consists in that the anisotropy of the experimentally observed microscale patterns is attributed only to the adsorbate diffusion which is, actually, not the same in the [001] and [1$\bar{1}$0] directions. Figure 10 shows the $1 \times 1 \rightarrow 1 \times 2 \rightarrow 1 \times 1$ transition between the nanodomains when the wave passes along the [1$\bar{1}$0] axis. The width of the propagating 1×2 zone (microscale wave) is about 0.1–0.4 μm.

VII. CONCLUSIONS

Kinetic oscillations on a catalytic surface involve processes with widely separated spatial and temporal scales. It is not practical to use the same algorithm to model slow surface restructuring, on the one side, and relatively fast adsorption, surface diffusion and reaction involving the adsorbate, on the other side. Both are necessary ingredients of the mechanism of oscillation and pattern formation on the catalytic surface, and patterns developing on the μm scale strongly depend on nanoscale surface phase transition and roughening.

Our way to overcome the computational challenge presented by scale separation is to apply the MC algorithm to the motion of Pt atoms only, while using use the mean-field approximation for the CO coverage. The CO fraction on the surface is averaged over the entire nanodomain area. A simple linear dependence of Pt-Pt binding energy on the av-
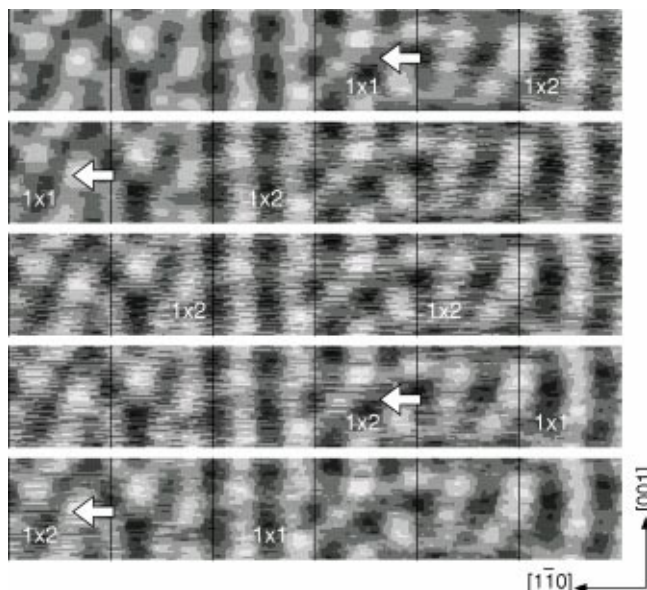
FIG. 10. Snapshots of nanodomains showing a propagating nanoscale $1\times1\rightarrow1\times2\rightarrow1\times1$ transition (a single traveling wave is shown).

eraged CO coverage, accounting also for different CO uptakes on different surface configurations, allows us to faithfully describe the reconstruction process, in qualitative agreement with the experiment.

Our simulations demonstrate that defect formation and roughening dominate the dynamics of surface phase transitions. The surface relaxation runs show that the 1×2 surface with defects reconstructs to more stable $1\times n$ superstructures. When the initial configuration has a sharp boundary between the 1×1 and 1×2 phases, this nanoscale front disintegrates due to the repeated phase transitions caused by CO coverage oscillations.

The Monte Carlo model coupled to phenomenological kinetic equation generates oscillations accompanied by reversible surface reconstruction. The repeated atomic transitions cause roughening and faceting of an originally flat surface. The oscillations period and amplitude are sensitive to the fraction of active top sites and to the value of CO uptake ratio k. A terraced surface has a reduced number of top atoms which can be involved in the reconstruction process. Mobility of the atoms on facet slopes is restricted; this may cause halt of oscillations on strongly roughened or terraced surface. An increase of k causes slower relaxation between the alternative surface phases and reduces roughening.

A spatial extension of the model including microscale CO diffusion reveals local synchronization of oscillations and formation of traveling waves. The propagation speed of the waves and wavelengths are insensitive to the surface anisotropy. The microscale anisotropy stems from the anisotropic CO diffusion. The propagating fronts separating the alternative surface phases develop on the CO diffusion scale, which is the characteristic scale of patterns observed in the experiments. This scale far exceeds the diffusion scale of Pt atoms, but the pattern formation as well as oscillations are sensitive to defects and roughening statistics governed by the short-scale processes.

Our model is qualitative, as it does not include activation barriers and realistic kinetics. It catches qualitative features of kinetic oscillations and dynamically induced roughening, but cannot reproduce order/disorder transition at high T. Computations taking into account activation barriers for single atomic jumps will be presented in a forthcoming communication.

[1] R. Imbihl and G. Ertl, Chem. Rev. **95**, 697 (1995).

[2] S. Jakubith, H.-H. Rotermund, W. Engel, A. von Oertzen, and G. Ertl, Phys. Rev. Lett. **65**, 3013 (1990).

[3] S. Nettesheim, A. von Oertzen, H.-H. Rotermund, and G. Ertl, J. Chem. Phys. **98**, 9977 (1993).

[4] F. Mertens and R. Imbihl, Nature (London) **370**, 124 (1994).

[5] R.A. van Santen, *Theoretical Heterogeneous Catalysis* (World Scientific, Singapore, 1991).

[6] T. Gritsch, D. Coulman, R.J. Behm, and G. Ertl, Phys. Rev. Lett. **63**, 1086 (1989).

[7] S. Schwegmann, W. Tappe, and U. Korte, Surf. Sci. **334**, 55 (1995).

[8] R.K. Sharma, W.A. Brown, and D.A. King, Surf. Sci. **414**, 68 (1998).

[9] K. Krischer, M. Eiswirth, and G. Ertl, J. Chem. Phys. **96**, 9161 (1992).

[10] I.K. Robinson, P.J. Eng, C. Romainczyk, and K. Kern, Surf. Sci. **367**, 105 (1996).

[11] P. Fery, W. Moritz, and D. Wolf, Phys. Lett. B **38**, 7275 (1988).

[12] M.A. Krzyzowski, P. Zeppenfeld, C. Romainczyk, R. David, G. Comsa, K.E. Kuhnke, and K. Kern, Phys. Rev. B **50**, 18 505 (1994).

[13] J. Falta, R. Imbihl, M. Sander, and M. Henzler, Phys. Rev. B **45**, 6858 (1992).

[14] M. Sander, R. Imbihl, and G. Ertl, J. Chem. Phys. **97**, 5193 (1992).

[15] R. Imbihl, Mod. Phys. Lett. B **6**, 493 (1992).

[16] J. Falta, R. Imbihl, and M. Henzler, Phys. Rev. Lett. **64**, 1409 (1990).

[17] M. Sander and R. Imbihl, Surf. Sci. **255**, 61 (1991).

[18] K.C. Rose, B. Berton, R. Imbihl, W. Engel, and A.M. Bradshaw, Phys. Rev. Lett. **79**, 3427 (1997).

[19] M.D. Graham, M. Bär, I.G. Kevrekidis, K. Asakura, J. Lauterbach, H.-H. Rotermund, and G. Ertl, Phys. Rev. E **52**, 76 (1994).

[20] M. Bär, N. Gottschalk, M. Eiswirth, and G. Ertl, J. Chem. Phys. **100**, 1202 (1994).

[21] L.M. Pismen, R. Imbihl, B.Y. Rubinstein, and M.I. Monin, Phys. Rev. E **58**, 2065 (1998).

[22] N. Gottschalk, F. Mertens, M. Bär, M. Eiswirth, and R. Imbihl, Phys. Rev. Lett. **73**, 3483 (1994).

[23] F. Mertens, N. Gottschalk, M. Bär, M. Eiswirth, A. Mikhailov, and R. Imbihl, Phys. Rev. E **51**, R5193 (1995).

[24] C.P. Schenk, M. Or-Guil, M. Bode, and H.-G. Purwins, Phys. Rev. Lett. **78**, 3781 (1997).

[25] M. Bär, A. Hagberg, E. Meron, and U. Thiele, Phys. Rev. Lett. **83**, 2664 (1999).

[26] E. Meron, M. Bär, A. Hagberg, and U. Thiele, Catal. Today **70**, 331 (2001).

[27] L.M. Pismen, Phys. Rev. Lett. **86**, 548 (2001).

[28] E. Meron, Phys. Rev. B **218**, 1 (1992).

[29] R.E. Goldstein, D.J. Muraki, and D.M. Petrich, Phys. Rev. E **53**, 3933 (1995).

[30] L.M. Pismen and B.Y. Rubinstein, Chaos **9**, 55 (1999).

[31] M. Monine, L.M. Pismen, M. Bär, and M. Or-Guil, J. Chem. Phys. **117**, 4473 (2002).

[32] R. Imbihl, A.E. Reynolds, and D. Kaletta, Phys. Rev. Lett. **67**, 275 (1991).

[33] P. Thostrup, E. Christoffersen, H.T. Lorensen, K.W. Jacobsen, F. Besenbacher, and J.K. Norskov, Phys. Rev. Lett. **87**, 126102 (2001).

[34] R.J. Gelten, A.P.J. Jansen, R.A. van Santen, J.J. Lukkien, J.P.L. Segers, and P.A.J. Hilbers, J. Chem. Phys. **108**, 5921 (1998).

[35] V.P. Zhdanov and B. Kasemo, J. Chem. Phys. **114**, 5351 (2001).

[36] K. Binder and D. W. Heermann, *Monte-Carlo Simulation in Statistical Physics*, 2nd ed. (Springer-Verlag, Berlin, 1992).

[37] D.P. Landau and K. Binder, *A Guide to Monte-Carlo Simulation in Statistical Physics* (Cambridge University Press, Cambridge, 2000).

[38] Kinetic Monte Carlo studies on the base of data extracted from STM experiments and density function theory calculations, Refs. [33,41–47].

[39] M. Monine and L.M. Pismen, Catal. Today **70**, 311 (2001).

[40] W.H. Press, S.A. Teukolsky, W.T. Vetterling, and B.P. Flannery, *Numerical Recipes*, 2nd ed. (Cambridge University Press, Cambridge, 1992).

[41] P.J. Feibelman, Phys. Rev. B **61**, R2452 (1999).

[42] T.R. Linderoth, S. Horch, L. Petersen, S. Helveg, M. Schønning, E. Lægsgaard, I. Stensgaard, and F. Besenbacher, Phys. Rev. B **61**, R2448 (1999).

[43] T.R. Linderoth, S. Horch, L. Petersen, S. Helveg, E. Lægsgaard, I. Stensgaard, and F. Besenbacher, Phys. Rev. Lett. **82**, 1494 (1999).

[44] T.R. Linderoth, S. Horch, E. Lægsgaard, I. Stensgaard, and F. Besenbacher, Phys. Rev. Lett. **78**, 4978 (1997).

[45] T.R. Linderoth, S. Horch, E. Lægsgaard, I. Stensgaard, and F. Besenbacher, Surf. Sci. **402**, 308 (1997).

[46] F. Montalenti and R. Ferrando, Phys. Rev. Lett. **82**, 1498 (1999).

[47] U. Kürpick, Phys. Rev. B **63**, 045409 (2001).